CHEMISTRY
A European Journal

A Journal of
ChemPubSoc Europe

Accepted Article

Title: Crystal Structures of Diaryliodonium Fluorides and their Implications for Fluorination Mechanisms

Authors: Yong Sok Lee, Joong-Hyun Chun, Milan Hodošček, and Victor Pike

To be cited as: *Chem. Eur. J.* 10.1002/chem.201604803

Link to VoR: http://dx.doi.org/10.1002/chem.201604803

Supported by
ACES

WILEY-VCH

10.1002/chem.201604803

Crystal Structures of Diaryliodonium Fluorides and their Implications for Fluorination Mechanisms

Yong-Sok Lee,[a] Joong-Hyun Chun,[b,d] Milan Hodošček,[c] and Victor W. Pike[b]

[a] *Center for Molecular Modeling, Office of Intramural Research, Center for Information Technology, National Institutes of Health, Building 12A, Rm 2049, Bethesda, MD 20892, United States*

[b] *Molecular Imaging Branch, National Institute of Mental Health, National Institutes of Health, Rm. B3C346A, 10 Center Drive, Bethesda, MD 20892, United States*

[c] *National Heart, Lung and Blood Institute, National Institutes of Health, Bethesda, MD 20892, United States, and National Institute of Chemistry, Ljubljana, Slovenia*

[d] *Present address: Department of Nuclear Medicine, Yonsei University College of Medicine, 50-1 Yonsei-ro, Seodaemun-gu, 03722, South Korea*

Abstract: The radiofluorination of diaryliodonium salts is of value for producing radiotracers for positron emission tomography. We report crystal structures for two diaryliodonium fluorides. Whereas diphenyliodonium fluoride (**1a**) exists as a tetramer bridged by four fluoride ions, 2-methylphenyl(phenyl)iodonium fluoride (**2a**) forms a fluoride-bridged dimer that is further halogen-bonded to two other monomers. We discuss the topological relationships between the two and their implications for fluorination in solution. Both radiofluorination and NMR spectroscopy show that thermolysis of **2a** gives 2-fluorotoluene and fluorobenzene in a 2 to 1 ratio that is in good agreement with the ratio observed from the radiofluorination of 2-methylphenyl(phenyl)iodonium chloride (**2b**). The constancy of the product ratio affirms that the fluorinations occur via the same two rapidly interconverting transition states whose energy difference dictates chemoselectivity. From quantum chemical studies with density functional theory we attribute the 'ortho-effect' to the favorable electrostatic interaction between

the incoming fluoride and the *o*-methyl in the transition state. By utilizing the crystal structures of **1a** and **2a**, the mechanisms of fluoroarene formation from diaryliodonium fluorides in their monomeric, homodimeric, heterodimeric, and tetrameric states were also investigated. We propose that oligomerization energy dictates whether the fluorination occurs through a monomeric or an oligomeric pathway.

Introduction

Diaryliodonium salts (Ar_2IX; diaryl-λ_3-iodanes) are hypervalent iodine compounds that have found extensive applications in synthetic organic chemistry, including use as arylating agents, oxidizing agents, and photoinitiators for polymerization.[1] These salts are reactive towards a variety of organic and inorganic nucleophiles.[2] Of particular interest is their reactivity towards cyclotron-produced [^{18}F]fluoride ion ($t_{1/2}$ = 109.8 min),[3] an important radioisotope for labeling radiotracers used in molecular imaging with positron emission tomography (PET), a powerful clinical and biomedical research tool.[4] The radiofluorination of diaryliodonium salts is among few metal-free methods that may use [^{18}F]fluoride ion to radiofluorinate electron-rich or electron-poor arenes at any desired ring position.[5,6] Consequently, this methodology finds increasing application for direct late-stage labeling of small-molecule radiotracers[7] and also for the preparation of monofunctionalized [^{18}F]fluoroarenes as synthons[8] for labeling structurally more complex radiotracers, such as proteins (Figure 1). Prominent examples of radiotracers prepared directly by this method include [^{18}F]flumazenil,[7b] [^{18}F]4-fluoro-*m*-hydroxyphenethylguanidine,[7d] [^{18}F]FIMX,[7e] and [^{18}F]UCB-H[7i] (Figure 1). Mechanistic details on the radiofluorination of diaryliodonium salts are nonetheless lacking. Improved mechanistic understanding might be informative on the design of higher-performing diaryliodonium salts as substrates in future PET radiotracer development.

a) Radiolabeling synthons:

R
= 4-Br
= 2-, 3- or 4-CH_2Cl
= 2-, 3- or 4-CH_2Br
= 3- or 4-CHO
= 2-, 3- or 4-CH_2N_3

X = 2-Cl, 2-Br, 6-Cl or 6-Br for 3-[^{18}F]
X= 5-Br, 6-Cl or 6-Br for 2-[^{18}F]

---

b) PET radiotracers:

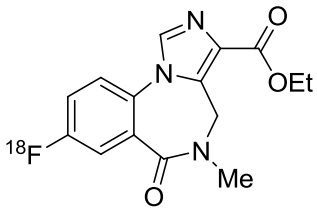

[^{18}F]flumazenil

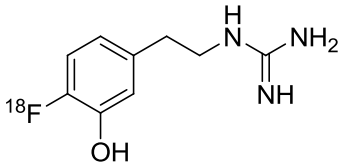

[^{18}F]4-fluoro-*m*-hydroxyphenethylguanidine

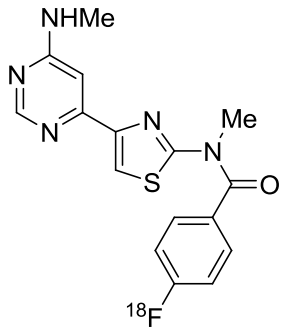

[^{18}F]FIMX

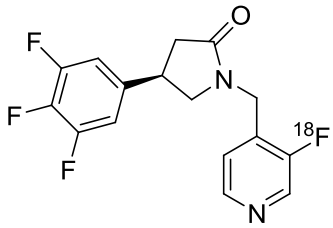

[^{18}F]UCB-H

Figure 1. Examples of a) radiolabeling synthons and b) prominent PET radiotracers produced directly by the radiofluorination of diaryliodonium salts.

Diaryliodonium salts are fluxional T-shaped molecules in which aryl rings rapidly switch axial and equatorial positions in trigonal bipyramidal geometry, a process described as pseudorotation. Radiofluorination reactions under metal-free conditions are usually presumed to proceed through the general pathway enunciated for reactions of nucleophiles (Nu^-) with diaryliodonium salts (Scheme 1), namely through ligand exchange followed by ligand coupling to either aryl ring with reductive elimination of aryl iodide.[9] Direct nucleophilic aromatic substitution (S_NAr) on an ipso carbon atom has also been suggested for several nucleophiles,[2a,2d,2f,2i,2m,3] including [^{18}F]fluoride ion.[3] Clearly, diaryliodonium

salts with identical aryl rings react with nucleophiles to give a single product (ArNu), whereas a salt with dissimilar aryl rings (ArIAr'X) may give two products (ArNu and Ar'Nu). Generally, however unsymmetric salts (Ar ≠ Ar') are much easier to prepare than symmetric salts, and in their synthetic applications for the arylation of nucleophiles provide for easier product separations from aryl iodide byproduct.[1a,10] From a radiosynthesis standpoint, an understanding of the mechanistic features that control the ratio of the two possible [^{18}F]fluoroarene products is desirable to avoid wastage of radioactivity and to simplify product purifications.

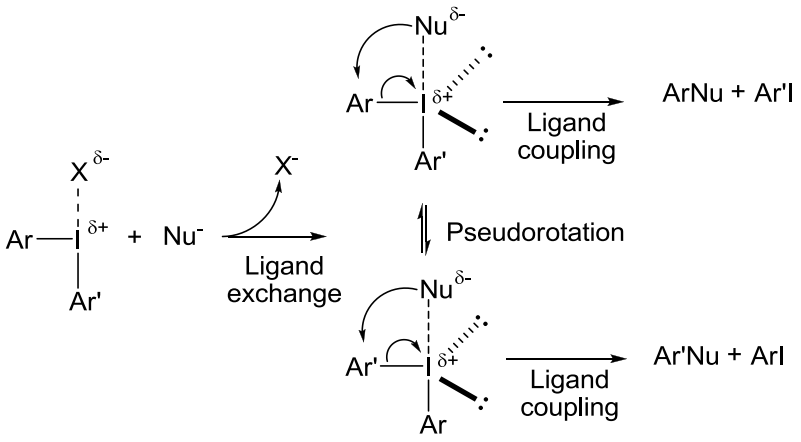

Scheme 1. General scheme for the reaction between diaryiodonium salts and nucleophiles.

In the absence of a substituent ortho to either carbon bonded to the hypervalent center, diaryliodonium salts react with nucleophiles to couple the nucleophile to the least electron-rich ring.[1a, 2d,3a,3b,,11] This has been well exemplified for [^{18}F]fluoride ion as nucleophile.[3b,11] Thus, fluorination chemoselectivity for aryl(2-thienyl)iodonium bromides has been correlated with the Hammett σ constant of the substituent in the electron-deficient aryl ring.[3b] For halide nucleophiles, *o*-alkyl substituents frequently promote preferential ligand coupling to the ortho substituted ring, even when this ring may be more electron-rich than the partner aryl ring.[3c,12] Again, this has been studied with [^{18}F]fluoride ion as nucleophile.[3c]

Various explanations have been proposed for the 'ortho effect' in the reactions of nucleophiles with diaryliodonium salts. The earliest of these explanations was that the *o*-methyl group imparted strain in the transition state of an aromatic nucleophilic substitution reaction, thereby promoting extrusion of the iodide of the partner aryl group.[12a] Subsequently a steric effect in a trigonal bipyramidal intermediate

having the nucleophile in apical position was considered responsible. The equatorial position in such an intermediate was considered to be less crowded than the apical position.[12b] Therefore, in cases where an *o*-substituted aryl ring is more bulky than its aryl partner, the *o*-substituted ring was expected to prefer the equatorial position and to be more available for ligand coupling.[12b] However, subsequent findings are not entirely consistent with this mechanistic model. For example Malmgren et al.[2k] found that the introduction of two *o*-alkyl groups on the same ring actually inverts chemoselectivity for reactions of diaryliodonium salts with malonate, a carbon nucleophile, an effect they dubbed an 'anti ortho effect'. Also the same diaryliodonium salts treated with a nitrogen nucleophile, namely aniline, failed to show an ortho effect. In their work Malmgren et al.[2k] found that *o*-methoxy substituents did not exert ortho effects. Limited data suggest that this is also true of *o*-methoxy groups in radiofluorination.[3c]

Clearly, questions remain with respect to understanding the unusual mechanistic influence of substituents placed in ortho position to the hypervalent iodine atom, especially with regard to control of chemoselectivity. Computational studies can be of value for understanding experimental findings and for gaining deeper mechanistic insights. Few computational studies have been performed that are relevant to the reactions of diaryliodonium salts with nucleophiles.[2k,13] In general, they support the general tandem ligand exchange-ligand coupling model described in Scheme 1. For example, Malmgren et al.[2k] performed density functional theory (DFT) calculations and these supported the ligand coupling mechanism and well predicted the chemoselectivities seen in their experiments on the reactions of various nucleophiles with diaryliodonium salts. One recent computational study[13d] has found that differences in partial charge between the ipso carbons of the aryl ligands correlated well with chemoselectivity for meta- and para-substituted diaryliodonium salt reactions with azide. However, this was not so for ortho-substituted salts. Another study[13e] concluded from DFT computations that the chemoselectivity of the reaction of [^{18}F]fluoride ion with diaryliodonium salts is controlled by transition state energy difference, as was much earlier suggested based on ab initio and MNDO-d SCF-MO computations on extrusion reactions of R_2I-F intermediates generated from disubstituted dialkynyl iodonium salts.[13a] This and a

subsequent study[13b] strongly alluded to a possible role for salt oligomers that has not received any subsequent attention, except recently for the radioiodination and astatination of diaryliodonium salts.[2m]

Here we aimed to gain deeper insights into aspects of the mechanism of the radiofluorination of diaryliodonium salts, including the possible role of oligomers, in order to provide a more rational basis for further application of this radiolabeling method to the development of new PET radiotracers. A key question was the structure of diaryliodonium salts in organic solution, because this knowledge is essential for formulating an understanding of the radiofluorination process, which is typically conducted in a polar aprotic solvent such as acetonitrile, *N*,*N*-dimethylformamide (DMF), or DMSO.[3,5a] In this regard, X-ray crystallography can provide important clues to solution structure. A few structures of crystalline diaryliodonium salts have been published and these show the capacity of salts to exist as oligomers connected by anion bridges.[14] However, to our knowledge the solid-state structure of any example of a diaryliodonium fluoride (Ar_2IF), which would be particularly relevant to our interest, has not been reported hitherto. The fluoride ion is special among the halide ions because of the strong electronegativity of the fluorine atom, its strong propensity to hydrate or, on the contrary, to show high nucleophilicity in naked form.[5a]

Herein, we report the crystal structures of two diaryliodonium fluorides, **1a** and **2a** (Figure 2). Based on these crystal structures, quantum chemical analyses were performed on the fluorides **2a**, **3a**, **4a**, **7** and **8** in monomeric conformation to elucidate the origin of the 'ortho effect'. We also investigated the mechanisms for the fluorination for diaryliodonium salts in monomeric, homodimeric, heterodimeric, and tetrameric states at the level of B3LYP/DGDZVP in order to assess the micro-environmental effect on the fluorination activation energy (E_a), as well as the feasibility of fluorination occurring in oligomeric states.

10.1002/chem.201604803

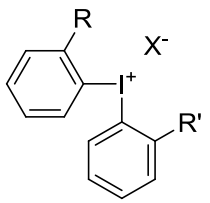

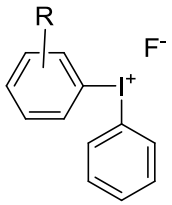

1a, R = R' = H, X^- = F^-
1b, R = R' = H, X^- = Cl^-
1c, R = R' = H, X^- = Br^-
1d, R = R' = H, X^- = I^-
2a, R = H, R' = Me, X^- = F^-
2b, R = H, R' = Me, X^- = Cl^-
2c, R = H, R' = Me, X^- = Br^-
2d, R = H, R' = Me, X^- = I^-
2e, R = H, R' = Me, X^- = OTs^-
3a, R = H, R' = OMe, X^- = F^-
4a, R = Me, R' = OMe, X^- = F^-
4b, R = Me, R' = OMe, X^- = Cl^-
5, R = R' = Me, X^- = Cl^-
6, R = R' = OMe, X^- = Cl^-

7, R = *m*-Me
8, R = *p*-Me

Figure 2. Diaryliodonium salts discussed and referred to in this study.

Results and Discussion

X-ray structures of diphenyliodonium fluoride and 2-methylphenyl(phenyl)iodonium fluoride

Diphenyliodonium fluoride (**1a**) and 2-methylphenyl(phenyl)iodonium fluoride (**2a**) (Figure 1) were prepared by literature methods. For example, commercially available diphenyliodonium tosylate was first converted into diphenyliodonium iodide (**1d**) in aqueous acetonitrile by anion metathesis with potassium iodide,[3c] followed by reaction with silver(I) oxide and then acidification with 10% aqueous hydrogen fluoride solution[15] (see Supporting Information). Single crystals of **1a** and **2a** were then obtained by the slow evaporation of their acetonitrile solutions in plastic vials.

Unlike the standard halide-bridged dimeric crystal structures of the higher halide salts Ph_2IX (X = Cl, Br, or I; **1b**–**1d**),[14] the fluoride salt **1a** crystallized as a tetrameric structure featuring an eight-membered ring held together by secondary I···F bonds having an average length of 2.545 Å (Figure 3). Isomorphic eight-membered rings have also been observed for $(p\text{-}MeC_6H_4)_2IBr$[14b] and XeF_6[16] in which $(p\text{-}MeC_6H_4)_2I^+$ and XeF_5^+ form a secondary bond to the respective Br^- and F^- species. These crystal structures, together with the previous characterization of a tetrameric cluster of 2-methylphenyl(2'-

methoxyphenyl)iodonium chloride (**4b**) in acetonitrile by LC-MS/MS,[14e] strongly indicate that tetrameric diaryliodonium fluorides can be stable structures, even in solution. An eight-membered I—F ring has also been seen in the crystal structure of 2-difluoroiodo-5-*tert*-butylxylene, which has two covalent I—F bonds of approximately equal length (average lengths = 2.019 Å and 1.991 Å).[17] However, in this difluoroiodo compound the average intermolecular I···F distance is longer at 2.93 Å; this is shorter than the sum of van der Waals radii of I and F (3.50 Å) but is 0.38 Å longer than the average I···F distance in **1a** (2.545 Å**)**. This comparison clearly indicates that the iodine-fluoride interaction in diaryliodonium fluorides is secondary bonding,[18] as has been reported also for the iodine-halide interactions in the crystal structures of **1b**–**1d**[14a] and of (*p*-$MeC_6H_4)_2IBr$.[14b]

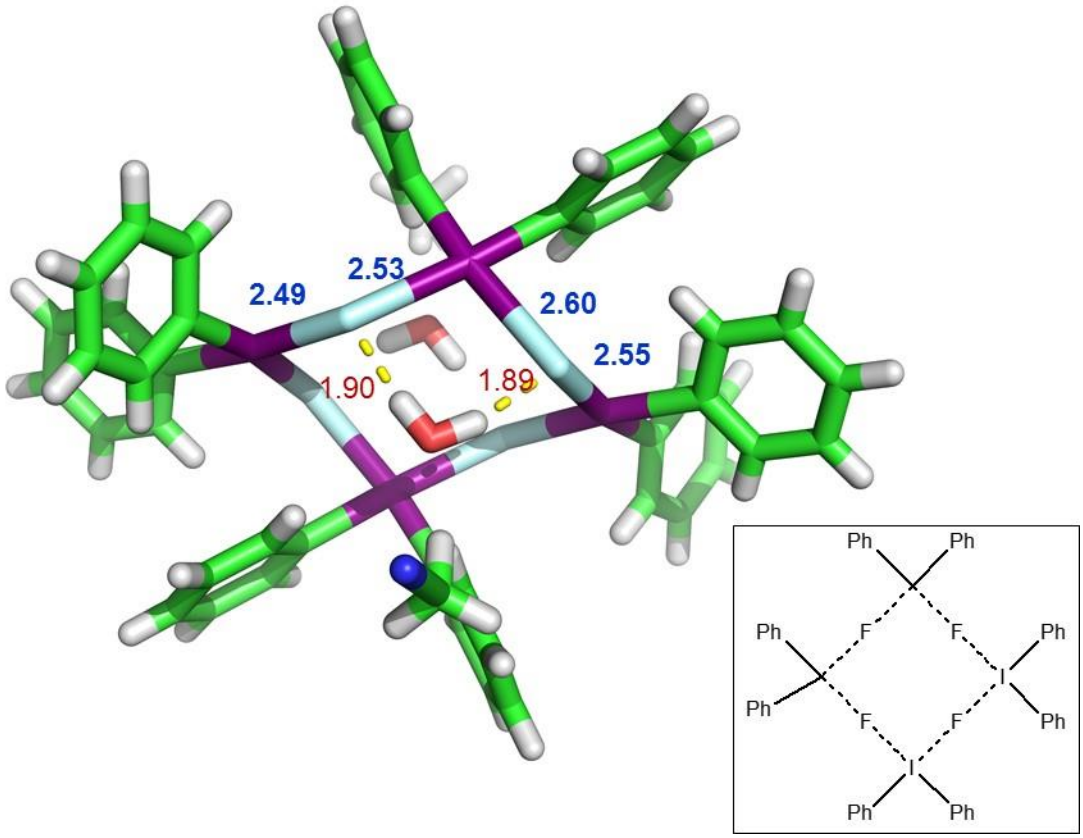

Figure 3. Crystal structure of **1a** together with the two water and two acetonitrile molecules from the crystallization solvent. Both bond lengths and H-bonding distances are shown in Å. Carbon atoms are shown in green, hydrogen atoms in white, oxygen atoms in red, iodine atoms in violet, nitrogen atoms in dark blue and fluorine atoms in gray. Blue distances are I···F bonds; red distances are H bonds. Since the unit cell has the center of inversion, only non-redundant bond distances are shown. The inset gives a formulaic planar view of the structure with water and acetonitrile molecules omitted.

Besides the eight-membered I···F ring of **1a**, the detailed crystal structure shows that each of the four bridging fluoride ions also forms a hydrogen bond (average F···H = 1.90 Å) with one of the two neighboring water molecules, each of which is also positioned to form a weak hydrogen bond with the methyl hydrogens of an acetonitrile molecule (Figure 3). The geometry optimization of **1a** at the level of B3LYP/DGDZVP in the gaseous phase gave 2.555 Å as the average I···F distance, the same as that seen in the crystal structure. The experimental and calculated average distances between the ipso carbon of the aryl ring and the fluoride ion are 3.10 Å and 3.14 Å, respectively. This close correspondence between the experimental and calculated structures for **1a** indicates that the structures of diaryliodonium fluorides can be investigated adequately at the level of B3LYP/DGDZVP.

The crystal structure of **2a** is another tetramer, but of a different kind. The central element is a fluoride-bridged dimer (Figure 4); its central iodine forms a secondary bond to each of the two bridging fluoride ions with an average I···F distance of 2.655 Å. This structure is notable in that each bridging fluoride ion has a further secondary bond to the iodine atom of a neighboring monomer (F···I = 2.56 Å). The distance between this iodine and the exocyclic fluoride ion is 2.54 Å, reflecting a weaker polarization of the exocyclic fluoride ion by two neighboring water molecules, which in turn hydrogen bond with a third water molecule. This third water molecule also hydrogen bonds with the second bridging fluoride ion of the dimer. The intricate hydrogen-bonding network in the crystal structure of **2a** gives three layers of square planarity, with the top and bottom layers each having three water molecules and one fluoride ion, and the middle layer having two iodine centers and two bridging fluoride ions.

10.1002/chem.201604803

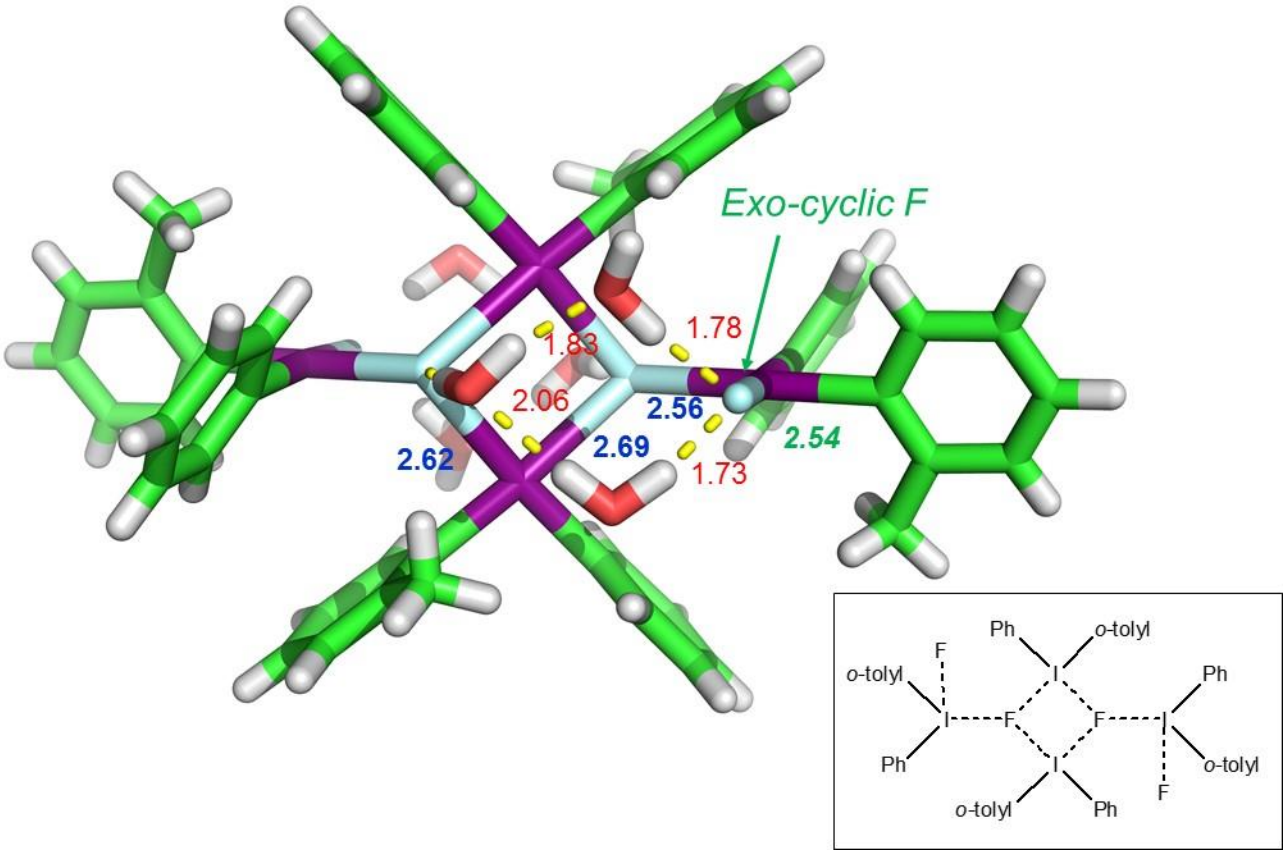

Figure 4. Crystal structure of **2a**. Hydrogen bonding interactions for three water molecules above and three water molecules below the plane of the two iodine and two fluorine atoms are indicated by their respective yellow dashed lines. Carbon atoms are shown in green, hydrogen atoms in white, oxygen atoms in red, iodine atoms in violet, and fluorine atoms in gray. Blue distances are I−F bonds; red distances are H bonds; green distance is an exocyclic I−F bond. All distances are in Å. The unit cell has the center of inversion and thus only non-redundant bond distances are given. The inset gives a formulaic planar view of the structure without water molecules.

The 2-methyl group in **2a** likely prevents the formation of the kind of tetramer seen for **1a** (Figure 3). Nevertheless, structure **2a** suggests a possibility for interconversion between the two types of tetramer. For example, the superposition of the iodine and fluorine atoms of **2a** onto **1a** indicates that the diaryl portion of **2a** can be fitted easily to that of **1a** by a simple translation and rotation (Figure 5). A tetrameric structure analogous to **1a** would then result when both iodine and fluorine atoms of **2a** move to their corresponding atom positions in **1a**.

10.1002/chem.201604803

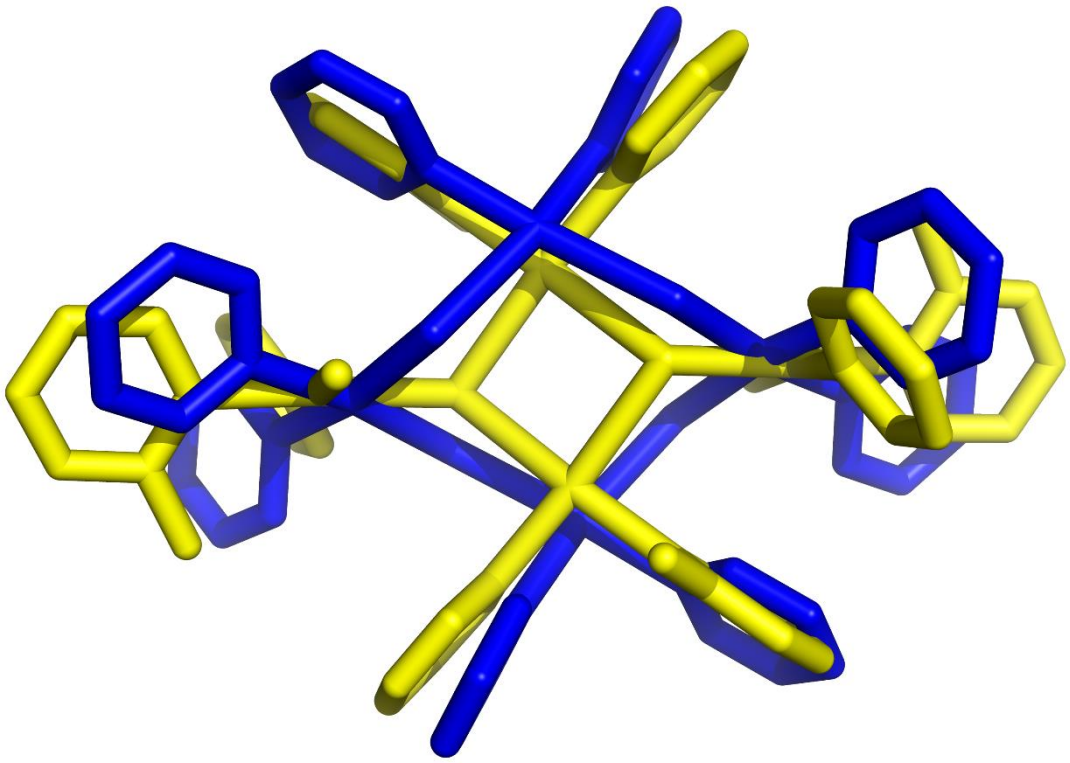

Figure 5. Overlay of the crystal structures of **1a** (dark blue) and **2a** (yellow); **2a** was superimposed with the best fit by using the four iodine and four fluorine atoms of **1a** as the common docking point. Hydrogen atoms and solvent molecules are not shown.

Experimental radiofluorination and fluorination

The fluorination of the unsymmetrical diaryliodonium fluoride **2a** occurs preferentially at the *o*-tolyl group. Thus, when **2a** and [^{18}F]fluoride ion of high molar activity were heated together in DMF at 180 ^{o}C for about 4 min, [^{18}F]*o*-fluorotoluene and [^{18}F]fluorobenzene was formed in 2.1 molar ratio (Scheme 2; Figure 6). Nearly identical fluoroarene product ratio was seen when **2a** was heated in DMSO-d_6 at 100 ^{o}C (Scheme 1), with the reaction monitored by ^{19}F NMR spectroscopy. The product NMR spectrum showed a major peak at δ –117.97 ppm for *o*-fluorotoluene and a minor peak at δ –113.23 ppm for fluorobenzene (Figure 7). As expected, a similar experiment on **1a** (δ –122.55 ppm) showed fluorobenzene (δ –113.12 ppm) to be the sole fluoroarene product.

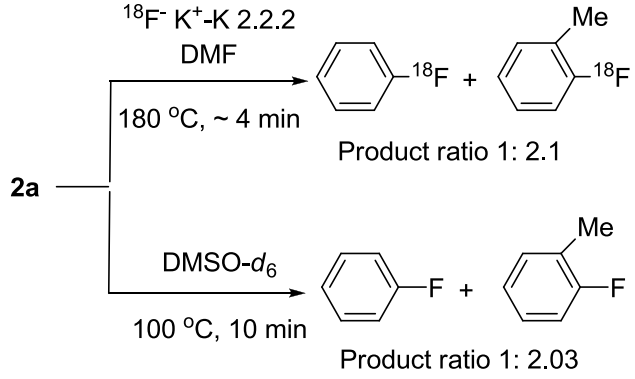

Scheme 2. Radiofluorination and thermolysis of **2a**.

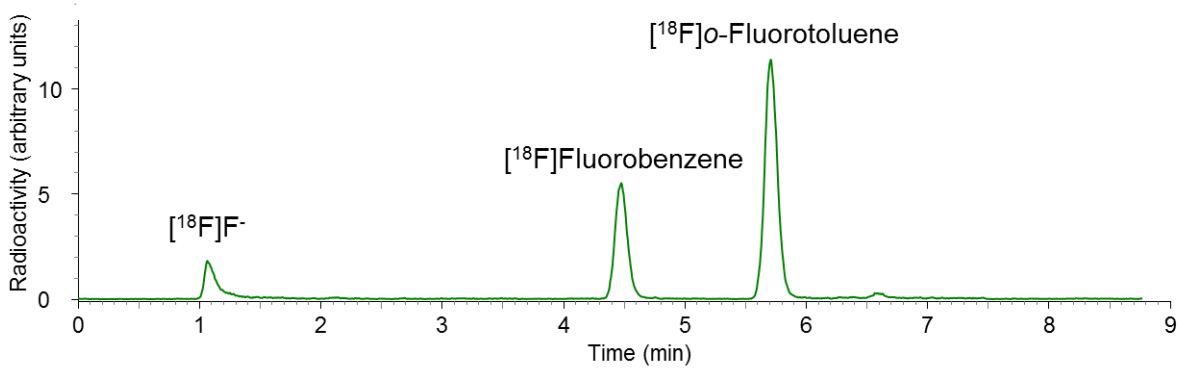

Figure 6. Reverse phase radio-HPLC chromatogram of the crude product from the radiofluorination of **2a**.

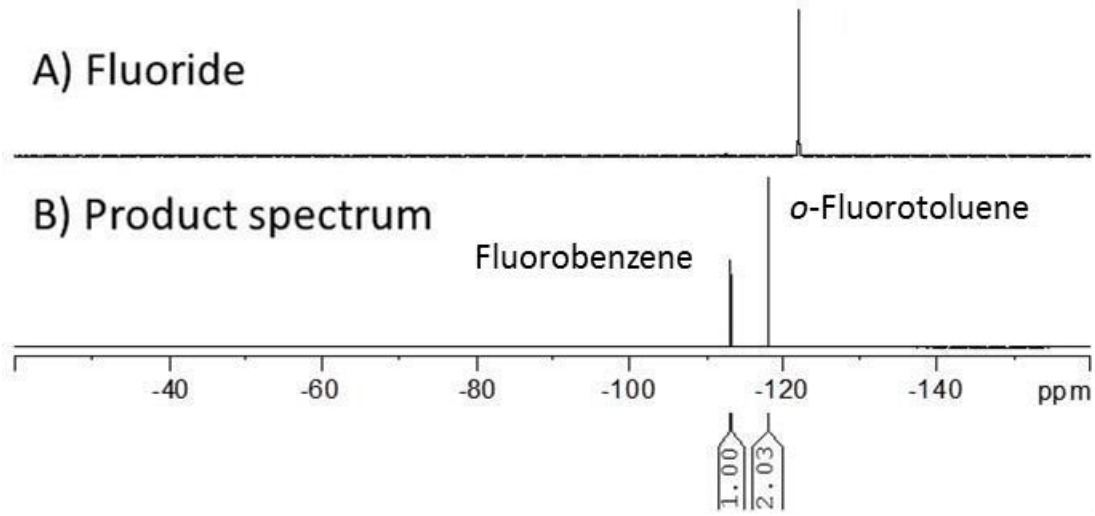

Figure 7. A) ^{19}F-NMR spectrum for **2a** in DMSO-d_6. B). ^{19}F NMR spectrum of the crude product from the thermal decomposition of **2a** in DMSO-d_6 at 100 °C for 10 min, showing the two fluoroarene products, fluorobenzene and *o*-fluorotoluene.

Fluorination mechanism in monomeric state

The product ratio (~ 2) from thermolysis of **2a**, detected with radiofluorination or ^{19}F-NMR spectroscopy,

is essentially idential to that reported in the radiofluorinations of 2-methylphenyl(phenyl)iodonium salts with Cl^-, Br, I^- or OTs^- as anion (**2b**–**2e)** in various solvents, including acetonitrile, acetonitrile-1.5% water, and DMF.[3c] This strongly indicates that the selectivities for the generation of fluorinated arenes from **2a–2e** under many different types of reaction conditions are very similar and are each dictated by the respective energy difference between the pair of transition states (*TS*s).

Based on crystal structure, quantum chemical study, and LC-MS evidence,[14e] the dimeric form of 2-methylphenyl(2'-methoxyphenyl)iodonium chloride (**4b**) is likely predominant in an organic solvent like acetonitrile. For diaryliodonium fluorides that may also show a tendency for such dimerization in solution, dissociation into monomers would be required before the secondary-bonded fluoride ion attacks an ipso aryl carbon atom. Because monomeric diaryliodonium salts are fluxional T-shaped molecules in which the two aryl rings may rapidly switch apical and equatorial positions, there are effectively two ground state (*GS*) structures.[1b,14e] In the case of a fluorination of a diaryliodonium salt with high molar activity [^{18}F]fluoride ion (i.e., of a non-fluoride salt precursor that is in vast excess over trace [^{18}F]fluoride ion), the [^{18}F]fluoride ion would first have to undergo ligand exchange with the anion (e.g., X^- = Cl^-, Br^-, I^- or $OTos^-$) bound to the central iodine atom in either of two rapidly interconverting monomers (Ar_2IX) before bonding to an ipso aryl carbon through either of two possible *TS*s. The energy difference between these two *TS*s has been proposed to control the ratio of the two fluoroarene products,[3c] in accord with the Curtin-Hammett principle.[19]

Figure 8 depicts a reacton path for the fluorination of monomeric **2a** in acetonitrile, derived from our quantum chemical analysis. In this reaction path, the interconversion energy barrier (TS_{int}) between the two *GS* conformers is 13.1 kcal/mol, which is substantially lower than the energy barriers for the formation of fluorobenzene via TS_A (20.0 kcal/mol) or *o*-fluorotoluene via TS_B (19.1 kcal/mol) (Table 1). The $\geq$ 6 kcal/mol difference between the TS_{int} and the TS_A or TS_B assures that the fluorination selectivity is dictated solely by the energy difference between TS_A and TS_B. As an example, the calculated product ratio (*o*-fluorotoluene/fluorobenzene) at 383.15 K is $\exp((-G_{TSB} + G_{TSA})/RT)$, equalling 3.3, which is in

fair agreement with the experimentally observed selectivity (2.3–3.0) for [^{18}F]*o*-fluorotoluene as the main product in the radiofluorination of (2-methylphenyl)(phenyl)iodonium salts (**2b**–**2e**) in acetonitrile containing 1.5% water.[3c] Whereas the GS_A conformer of **2a** is 0.3 kcal/mol more stable than the GS_B conformer, the energetics reverses in the *TS*s making the TS_B more stable by 0.9 kcal/mol than the TS_A. In the experimental case, the presence of 1.5% water would ensure that the [^{18}F]fluoride ion was fully hydrated.[20] These waters of hydration would need to be shed during the radiofluorination reaction. This process was not taken into account in the computed pathway. Nonetheless, computations have shown how solvated fluoride ion can serve as a good nucleophile despite its very high solvation energy.[20b] The close agreement between the experimental and computed fluorination selectivities implies that fluoride ion dehydration had little impact on reaction energetics and outcome. The experimental reaction milieu also included K^+-K.2.2.2 complex plus carbonate, and likewise their influences appear to have been negligible.

10.1002/chem.201604803

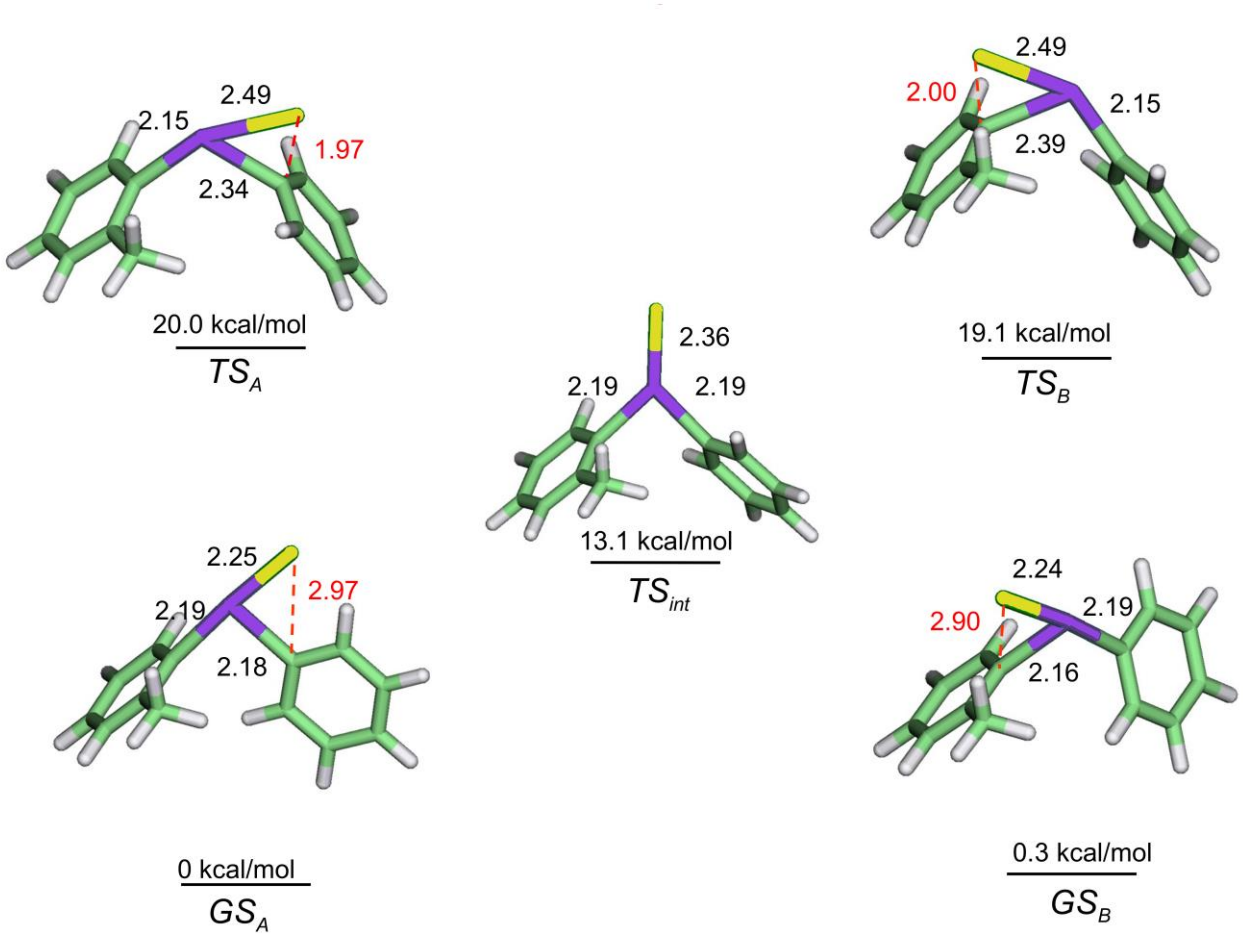

Figure 8. Reaction path for the thermolysis of monomeric **2a** in acetonitrile. Labeled bond distances are shown in Å. Carbon atoms are shown in green, hydrogen atoms in white, iodine atoms in violet, and fluorine atoms in yellow. Dashed red lines and numbers are distances between the fluoride ion and the nearest carbon atom ipso to the iodine atom. *TS*$_A$ leads to fluorobenzene and *TS*$_B$ to *o*-fluorotoluene.

Table 1. Calculated relative ΔG (kcal/mol) at the level of B3LYP/DGDZVP for thermolysis of diaryliodonium fluorides in acetonitrile.

Structure[a]	Diaryliodonium fluoride			
	1a	**2a**	**3a**	**4a**
GS$_A$	0	0	0	1.1
GS$_B$	0	0.3	0.9	0
TS$_{Int}$	13.5	13.1	13.9	13.6
TS$_A$	19.8	20.0	20.2	20.8
TS$_B$		19.1	21.9	18.6

[a] *TS*$_A$ leads to fluorobenzene. *TS*$_B$ leads to *o*-fluorotoluene for **2a** and to *o*-fluoroanisole for **3a** and **4a**. Energetics were calculated for **1a** at 298.15 K, **2a** at 383.15 K, and **3a** and **4a** at 413.15 K.

Origin of the ortho effect

The spatial positions of the fluoride ion in the *TS*s of **2a**, as shown in Figure 8, provide insight into their relative stabilities. For example, the fluoride ion in *TS*$_B$ is positioned 2.00 Å away from the ipso aryl

carbon as compared to 1.97 Å in TS_A. Nonetheless, such a difference is too small to explain the widely observed 'ortho effect' imparted by an *o*-alkyl group in the reaction of diarylodonium salts with various nucleophiles,[2h,2m,3c,12] where this effect may be described as the greater tendency of an *o*-alkyl group over an *o*-hydrogen atom to favor ligand binding at the ipso carbon of the same ring. In order to fully address the *o*-methyl effect, quantum chemical calculations were extended to both *m*-methyl (**7**) and *p*-methyl (**8**) substituted Ar_2IFs (Figure 2). The electronic energy of TS_B is lower than that of TS_A by 1.0 kcal/mol for **2a**. However, for **7** and **8**, the TS_A becomes more stable than the TS_B by 0.2 kcal/mol and 1.0 kcal/mol, respectively. These energy differences are in good agreement with the observed chemoselectivity for **8** favoring the formation of fluorobenzene over *p*-fluorotoluene by 2 to 1;[3a] no selectivity was observed for **7**.[11b] More importantly, the slight variations of the electronic energy differences between the two *TS*s depend upon the position of the methyl group in the arene, which in turn suggests that the origin of the *o*-methyl effect on selectivity is electrostatic (rather than solely inductive). To illustrate the electrostatic origin, both the atomic charge on the methyl group and the distance of this group from the fluoride were calculated for the TS_B of **2a**. The carbon of the *o*-methyl group is 3.15 Å away from the fluoride and this group has the atomic polar tensor (APT) derived charge of +0.12. By comparison, the respective carbons of the *m*-methyl group in the TS_B of **7a** and the *p*-methyl group in the TS_B of **8** are 5.07 Å and 5.84 Å from the fluoride respectively, and both methyl groups have the APT-derived charge of +0.01. This implies a 20-fold higher stability of the *o*-methyl over the *p*-methyl; the charge on F does not change much (see Supporting Information). Whereas the methyl group in any position donates its electrons to the aryl ring and likely raises the energy of the TS_B over the TS_A, at the same time the *o*-methyl is better positioned to lower the energy of the TS_B via direct charge interaction with the incoming fluoride. The electrostatic potential map for the TS_A and TS_B of **2a** (Figure S1) further illustrates the local field on the molecular surfaces.

For the unsymmetrical *o*-methoxy-substituted fluoride (**3a**), the GS_A conformation is more stable than the GS_B conformation (fluoride ion nearer to *o*-anisyl ring) by 0.9 kcal/mol (Table 1 and

Figure S1). The bulkiness of the *o*-methoxy group relative to the *o*-methyl group along with the high electron density on the oxygen atom of the former gives rise to a stronger electrostatic repulsion with the fluoride ion in the GS_B conformation (Figure S2). Therefore, unlike the *o*-methyl-substituted case (**2a**), the TS_A (20.2 kcal/mol) is 1.7 kcal/mol more stable than the TS_B (21.9 kcal/mol). The calculated fluorobenzene/*o*-fluoroanisole product ratio at 413.15 K is 0.12, which is also in good agreement with the observed fluoroarene product ratio of 0.11 in the radiofluorination of (2-methoxyphenyl)(phenyl)iodonium chloride (**3b**) in DMF-0.25% water.[3c] Qualitatively, the *o*-methoxy group donates electrons to the aryl ring and thus destabilizes the TS_B relative to the TS_A, as pointed out in the previous work of Ochiai et. al.[9a] Given that the distance between the fluoride and the methoxy oxygen atom in the TS_B is only 3.05 Å, the TS_B is further destabilized by the unfavorable electrostatic interaction between the two atoms. The electrostic potential map for the TS_A and TS_B of **3a** further illustrates this (Figure S3). The case of the fluoride substituted with *o*-methyl on one ring and with *o*-methoxy on the other (**4a**) can be rationalized similarly. The calculated ΔG diffference between the TS_A and TS_B is 2.2 kcal/mol (Figure S4) reflecting the stabilization of TS_B and destabilization of TS_A due to the respective *o*-methyl and *o*-methoxy group with resepct to the unsubstituted aryl ring. This difference is also in good agreement with the observed aryl ring fluorination selectivity of **4a** (2.4 kcal/mol). Our quantum chemical analysis of the effect of an *o*-methoxy group thus suggests that the *o*-anisyl group may serve as a generally effective spectator aryl group partner in the radiofluorination of diaryliodonium salts, in accord with some of our simple published examples.[3c] This observation can be put to good use in future PET radiotracer syntheses as a means to enhance the yield of desired radiotracer over unwanted radiofluorinated byproduct.

GS and *TS* in homodimeric, heterodimeric, and tetrameric states

Prior studies[3c,13a,13b] have also pointed out that the halogenation selectivity of aryl rings with regard to diaryliodonium salts in monomeric state is dictated by *TS* energy differences. However, the possibility for the fluorination of diaryliodonium salts in dimeric or tetrameric states has not yet been fully explored.

As earlier mentioned, the fluorination mechanism in oligomeric states was first discussed in the work of Martín-Santamaría et al.,[13b] but with regard to non-aromatic model oligomers, such as (I(CC-CN)(CC-OMe)F)$_2$, and not with regard to diaryliodonium salts in dimeric or tetrameric state. The present crystal structures of tetrameric **1a** and **2a** provide reliable descriptions of the *GS* conformations that otherwise might only be guessed at. Accordingly, we were well set to investigate the fluorination of **1a** and **2a** in their homodimeric, heterodimeric, and tetrameric states with the aim of assessing the environmental effects on their thermochemical feasibilities for existence in solution, their activation energies (E_as), and ring selectivities in radiofluorination. In the case of heterodimers, the dimeric structure of Ar_2IF was modified to construct the heterodimer (Ar_2IF)(Ar_2ICl).

Figure 9A depicts the alternation of the I—F distance from 2.40 Å to 2.78 Å in the dimer of **1a**, $(Ph_2IF)_2$. By comparison, the I—Cl distances in the dimer of **1b**, $(Ph_2ICl)_2$, are all comparable at 3.11 Å. The monomeric I—F and I—Cl distances were calculated to be significantly shorter at 2.25 Å and 2.86 Å, respectively. Thus, upon dimerization, the polarization induced by the neighboring monomer lengthens both the I—F and I—Cl distances. However, the bond length alternation in $(Ph_2IF)_2$ reflects that the fluoride ion is much less polarized than the chloride ion. Upon heterodimerization of Ph_2IF with Ph_2ICl (Table 2, Equation 3), the I—F bond lengthens to 2.53 Å, and the I—Cl bond to 3.18 Å (Figure 9B). In the homotetramer $(Ph_2IF)_4$ (Figure 9C), a slight I—F bond length alternation ranging from 2.47 Å to 2.53 Å occurs, suggesting that the tetrameric environment smoothes out the I—F bond length alternation seen in the homodimeric environment.

10.1002/chem.201604803

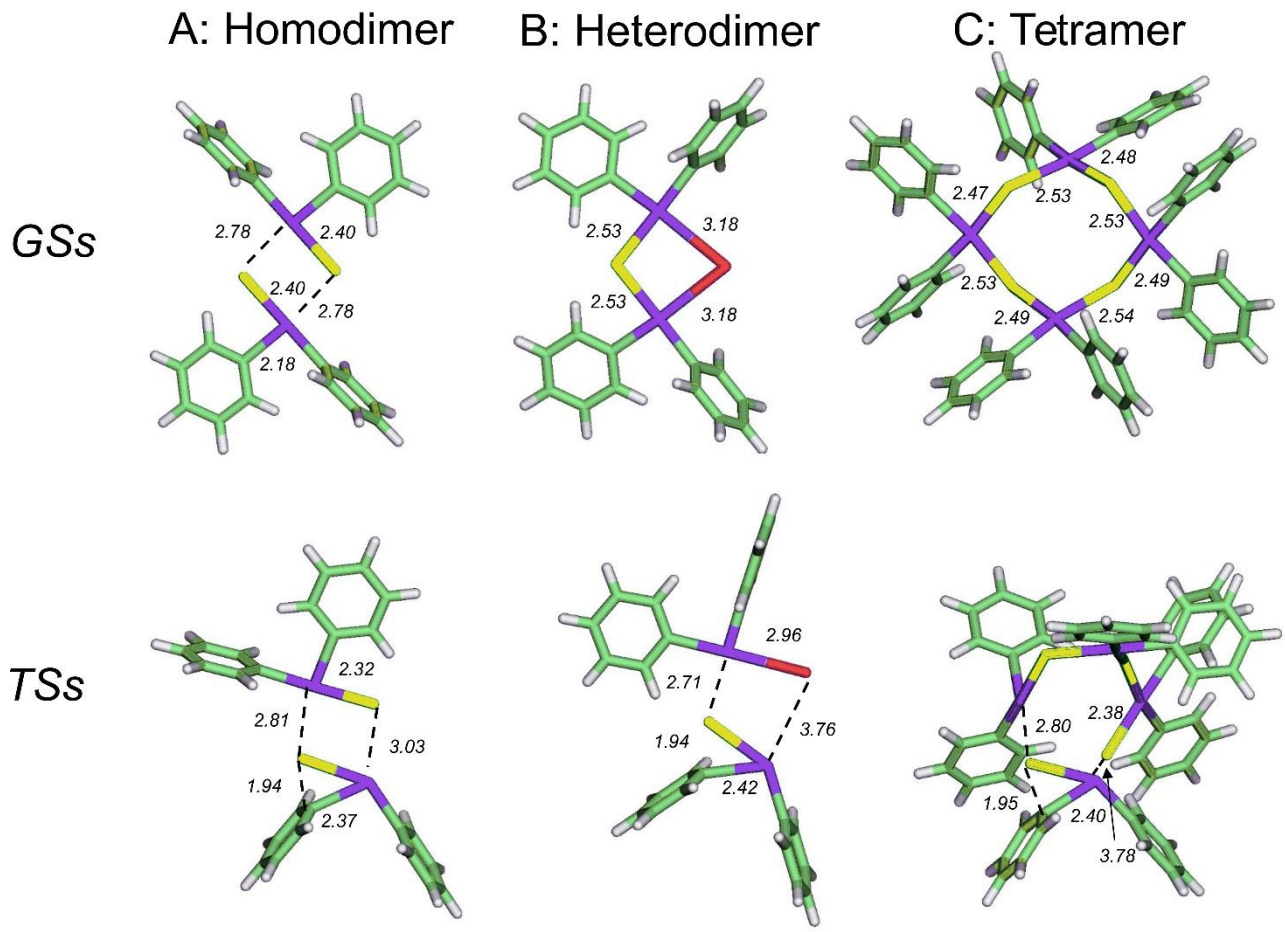

Figure 9. Structures of *GS*s and *TS*s of diphenyliodonium fluoride (**1a**) in dimeric, heterodimeric and tetrameric states. All distances are in Å. Carbon atoms are shown in green, hydrogen atoms in white, iodine atoms in violet, chlorine atoms in red, and fluorine atoms in yellow. The coordinates of these structures are given in the Supporting Information.

Enthalpies for homodimerization were calculated by subtracting the sum of the enthalpy of each monomer from that of the dimer at 298.15 K, giving values of –3.4 kcal/mol for the fluoride **1a** (Table 2, Equation 1) and –8.6 kcal/mol for the chloride **1b** (Table 2, Equation 2). These values are consistent with the aforementioned bond length alternation and/or polarization effects. For the formation of the heterodimer (Ph_2IF)(Ph_2ICl) from the monomers **1a** and **1b**, the ΔH value was calculated to be –8.0 kcal/mol (Table 2, Equation 3). The alternative formation of this dimer, through the exchange of the fluoride ion in potassium fluoride with a chloride ion in the dimer $(Ph_2ICl)_2$, was found to be thermochemically feasible. For this process (Table 2, Equation 4), the calculated ΔH and ΔG values are –7.9 kcal/mol and –7.1 kcal/mol, respectively. The enthalpy for the tetramerization of **1a** was calculated

to be – 14.7 kcal/mol (Table 2, Equation 5).

Table 2. Calculated *ΔH* and *ΔG* for iodonium salt dimer and tetramer formations in the reaction field of acetonitrile at 298.15 K.

Equation		*ΔH* (kcal/mol)	*ΔG* (kcal/mol)
1	$2Ph_2IF \rightarrow (Ph_2IF)_2$	–3.4	5.9
2	$2Ph_2ICl \rightarrow (Ph_2ICl)_2$	–8.6	1.4
3	$Ph_2IF + Ph_2ICl \rightarrow (Ph_2IF)(Ph_2ICl)$	–8.0	1.4
4	$(Ph_2ICl)_2 + KF \rightarrow (Ph_2IF)(Ph_2ICl) + KCl$	–7.9	–7.1
5	$4Ph_2IF \rightarrow (Ph_2IF)_4$	−14.7	16.6

Changes in enthalpy (*ΔH*) clearly favor dimers and tetramers over the respective monomers (Table 2). However, the calculated *ΔG* values for dimerization of **1a** (5.9 kcal/mol) (Table 2, Equation 1) and **1b** (1.4 kcal/mol) (Table 2, Equation 2), as well as for tetramerization of **1a** (16.6 kcal/mol) (Table 2, Equation 5) do not favor such cluster formation. For the formation of the heterodimer $(Ph_2IF)(Ph_2ICl)$ from monomers, the *ΔG* value was also calculated to have a small positive value (1.4 kcal/mol; Table 2, Equation 3). Such unfavorable *ΔG*s arise mainly from the the loss of the translational and rotational (TR) entropy of the two monomers. For example, this is 70 $calmol^{-1}K^{-1}$ or 35 *R* upon dimerization of **1a**, based upon the ideal gas approximation. However, the TR entropy contribution of a monomer to dimerization in solution is known to be much lower due to its restricted movement. As an example, the experimental TR entropy contribution to the dimerization of a protein in water was reported to be $5\,R \pm 4\,R$ as compared to 50 *R* from the ideal gas approximation used here.[21] Consequently, the actual *ΔG* values for dimerization or tetramerization of **1a** are expected to be more favorable than indicated in Table 2. In this regard, we note that small negative *ΔG* values of about 3 kcal/mol have been experimentally determined for the dimerization of 4,4'-dicyclohexyldiphenyliodonium iodide in benzene[2f] and also for (*Z*)-(*β*-bromoalkenyl)-(phenyl)iodonium bromide in chloroform.[22]

Fluorination via monomeric or oligomeric states

The calculated E_a value for fluorobenzene formation from **1a**, taken as the difference in the zero-point corrected energy between the *GS* and the *TS*, steadily increases from 19.8 kcal/mol for the monomer to

21.3 kcal/mol for the homodimer, and then to 23.1 kcal/mol for the heterodimer (Table 3). As seen in Figure 9A for the homodimer, the approach of the incoming fluoride ion to the ipso aryl carbon has to overcome an extra charge interaction provided by the second central iodine to form fluorobenzene. In the heterodimeric case (Figure 9B), this extra charge interaction is even stronger, because the I···F distance at the TS is 2.71 Å as compared to 2.81 Å for the homodimer (Figure 9A). In addition, the more polarizable electron cloud of chloride ion is likely to provide a better charge interaction to the central iodine undergoing thermolysis, resulting in a higher E_a value for fluorobenzene formation. Whereas heterodimers are likely predominant in the radiofluorination of the chloride **1b**, the thermolysis of the fluoride **1a** may involve the formation of homodimers or even homotetramers in solution. The E_a of the tetramer is 21.9 kcal/mol, which is 2.1 kcal/mol higher than that of the monomer. The E_a values calculated for the monomer, homodimer and tetramer fall in the range of the experimental E_a (20.9 ± 1.6 kcal/mol) measured previously for the high molar activity radiofluorination of **1b** in DMF.[3c] Also, the E_a (23.1 kcal/mol) of the heterodimer is only 0.6 kcal/mol above the range of the experimental value. Thus, this E_a comparison cannot distinguish clearly whether the major pathway for fluorination of **1a** is monomeric or oligomeric.

Table 3. E_a (kcal/mol)_and $\Delta G^{\ddagger}$ (kcal/mol) at 298.15 K for the production of fluoroarenes from diaryliodonium salt monomers and oligomers at the level of B3LYP/DGDZVP in acetonitrile.

	Salt [a]		*TS* type[b]	Monomer		Homodimer		Heterodimer		Tetramer		Experimental[c]
#	Substituents			E_a	$\Delta G^{\ddagger}$	E_a	$\Delta G^{\ddagger}$	E_a	$\Delta G^{\ddagger}$	E_a	$\Delta G^{\ddagger}$	E_a
1a	H	H	TS_A	19.8	19.8	21.3	20.2	23.1	21.8	21.9	21.5	20.9 ± 1.6
2a	H	2-Me	TS_A	20.1	19.9	21.6	21.0	23.4	22.7			23.5 ± 1.6
2a	H	2-Me	TS_B	18.7	18.9	21.1	20.5	22.0	21.0			18.3 ± 0.9
4a	2-Me	2-OMe	TS_B	18.7								25.1 ± 2.6
5	2-Me	2-Me	TS_B	17.6		20.9		22.0		23.5		27.5 ± 2.0
6	2-OMe	2-OMe	TS_B	20.8								28.0 ± 1.6

[a] In diphenyliodonium fluorides for monomer, homodimer and tetramer. Heterodimer is composed of the chloride monomer plus a fluoride monomer.
[b] TS_A leads to fluorobenzene; TS_B type leads to *o*-fluorotoluene product for **4a** and **5**, and to *o*-fluoroanisole for **6**.
[c] From reference [3c].

For **2a**, the E_as for fluorobenzene formation via TS_A in monomeric, homodimeric and heterodimeric environments remain very comparable to those of **1a** (Table 3), suggesting that the formation of

fluorobenzene is not affected by the presence of the *o*-methyl group on the other aryl ring. For *o*-fluorotoluene formation via TS_B, the E_a increases from 18.7 kcal/mol for the monomer to 21.1 kcal/mol for the homodimer and then to 22.0 kcal/mol for the heterodimer. The same rationale that was given for the increase in the E_a for **1a** across oligomers can be invoked to explain this trend. The presence of the *o*-methyl group results in TS_B values that are all lower than for reactions of **2a** or **1a** through TS_As. Whereas the E_a values for **2a** are 2.4–3 kcal/mol higher in the dimeric enviroment, their calculated selectivities based on $\Delta\Delta G^{\ddagger}$ at 298.15 K still favor the formation of *o*-fluorotoluene over fluorobenzene. We have also computationally investigated the formation of *o*-chlororotoluene via TS_B (E_a = 27.1 kcal/mol) and of chlororobenzene via TS_A (E_a = 28.4 kcal/mol); the ortho effect is still manifested in chlorination in agreement with experiment.[2h] More importantly, these higher calculated E_as (Figure S5) assure that the formation of fluorinated products occurs before the chlorination.

A reaction path for fluorination of **1a**/**1b** was constructed assuming that ΔG for the formation of $(Ph_2IF)_2$ or $(Ph_2IF)(Ph_2ICl)$ is favorable over their corresponding monomers (Figure 10). In this reaction path, the more stable dimer is in equilibrium with its monomers, and the interconversion between the two is much faster than the fluorination itself. For example, the dissociation of $(Ph_2IF)_2$ as a function of the inter-iodine distance (Figure S6) indicates that the ΔG at 298.15 K for the two monomers separated by the I---I distance of 7.5 Å is 9.1 kcal/mol less stable than the dimer separated by a distance of 4.0 Å. Whereas this value of 9.1 kcal/mol does not represent the *TS* energy between the dimer and its monomers in solution, it is substantially lower than the E_a for fluorination in both monomeric and dimeric **1a**. Note that the TS_M and TS_D in Figure 10 represent the *TS* of fluorination in monomeric and dimeric conformations, respectively, and their energy levels are depicted with respect to the *GS* of dimer (GS_D); TS_M energy level is the sum of the ΔGS_D and $\Delta G_M^{\ddagger}$ values of the monomeric **1a**.

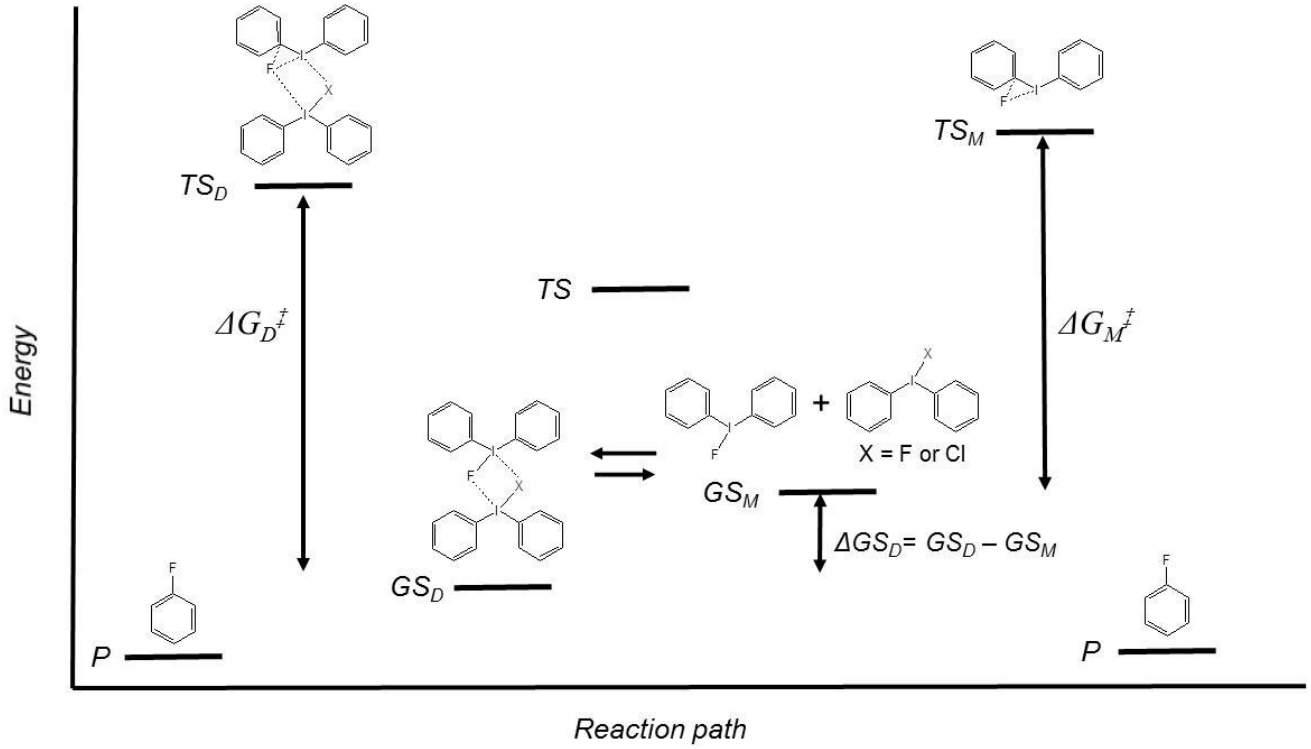

Figure 10. Reaction path for the fluorination of **1a**/**1b**. The more stable dimer is in equilibrium with its monomers, and the interconversion between the two is assumed to be much faster than the fluorination itself. The TS_M and TS_D represent the *TS* of fluorination in monomeric and dimeric conformations, respectively, and their energy levels are depicted with respect to the *GS* of dimer (GS_D); TS_M energy level is the sum of the ΔGS_D and $\Delta G_M^{\ddagger}$ values of the monomeric **1a**. The TS_M of the heterodimeric conformation does not show Ph_2ICl.

In the case of $(Ph_2IF)_2$, when the ΔGS_D is more negative than − 0.4 kcal/mol, the dimeric path to the TS_D of 20.2 kcal/mol will become a major path for the formation of fluorobenzene rather than the monomeric path with $\Delta G_M^{\ddagger}$ of 19.8 kcal/mol. For the fluorination to occur in the heterodimeric or tetrameric conformation, the dimerization or tetramerization energy then has to be more than 2 kcal/mol for the heterodimer or 1.7 kcal/mol for the tetramer. This will compensate for the increase in the $\Delta G^{\ddagger}$ in the heterodimer (21.8 kcal/mol) and the tetramer (21.5 kcal/mol). Nonetheless, the small differences in the $\Delta G^{\ddagger}$s values in Table 2 suggests that the fluorination of **1a** or **1b** likely occur in all conformations Only when the ΔG for dimerization or tetramerization is more negative than − 4 kcal/mol, will the dimeric or tetrameric pathway be the major pathway for the fluorination of diaryliodonium salts.

Figure 10 may also explain the discrepancy between the experimental and the calculated E_as. For compound **1a**, both the calculated E_a (19.8 kcal/mol to 23.1 kcal/mol) and the experimental E_a (20.9 ± 1.6 kcal/mol) are comparable. For the formation of fluorotoluene from **2a**, the calculated E_a for the monomer

(18.7 kcal/mol) is also comparable to the experimental E_a value for the correspondimg chloride **2b** (18.3 ± 0.9 kcal/mol).[3c] However, the experimental E_a value for the symmetrically *o*-methyl substituted diphenyliodonium chloride **5** (27.5 ± 2.0 kcal/mol) [3c] is substantially higher than the calculated E_a value, which ranges from 17.6 kcal/mol for the monomeric conformation to 23.5 kcal/mol for the tetrameric conformation (Table 3). The experimental E_a value for the unsymmetrically substituted diaryliodonium chloride **4** (25.1 ± 2.6 kcal; R = *o*-Me, R´ = *o*-OMe) as well as for the symmetrically *o*-methoxy substituted diphenyliodonium chloride **6** (28.0 ± 1.6 kcal/mol)[3c] are also higher than the calculated monomer E_a values that are 20.8 kcal/mol. This inconsistency can be rationalized when the dissociation of a dimer of a diaryliodonium fluoride (e.g., Figure 9A and Figure 9B) into two monomers is considered. Note that the ΔG at 298.15 K of the two monomers of **1a** separated by the I---I distance at 7.5 Å was calculated to be 9.1 kcal/mol less stable than the dimer at 4.0 Å. Accordingly, those reactions with the experimenal E_a value of ~ 27–28 kcal/mol may then arise from a reaction occurring in a concerted manner in which the dissociation of such dimer is coupled with the fluorination of the monomeric diaryliodonium iodide with an energy barrier of ~ 20 kcal/mol.

From a practical standpoint, a tendency for simple and complex diaryliodonium salts to adopt oligomeric states in solution may result in a range of amenabilities to undergo useful radiofluorinations, dependent on for example bridging anions and solvent. Such dependence has been well observed experimentally.[3c]

Conclusions

Diaryliodonium fluorides may exist in two types of tetrameric structure. An interconversion pathway between the two types of structure in solution appears feasible. Both the radiofluorination and thermolysis of the fluoride **2a** give the same fluoroarene product ratio as observed in the radiofluorination of the corresponding chloride **2b**. For this reaction, we constructed a reaction path for monomeric **2a** whose *TS* energy difference agrees with the experimental product ratio, and thus affirms the previous proposal that the fluoroarene product selectivity in the fluorination of diaryliodonium salts is dictated by the *TS* energy

differences. These findings also provide stronger insight into the detailed mechanism of the fluorinations of diaryliodonium salts, especially with regard to the electrostatic influence of the *o*-methyl substituent and spectator ring effects, and this may eventually find application in the design of more effective precursors for PET radiotracer synthesis. In addition, the fluorination of diaryliodonium salts may occur in both monomeric and oligomeric states depending upon the magnitude of the energy for salt dimerization or tetramerization. From this limited study it appears that ring selectivity for fluorination is quite insensitive to reaction pathway through monomers or oligomers.

Experimental

Quantum Chemistry. Quantum chemical calculations with the density functional theory were carried out using the B3LYP functional and DGDZVP basis set as implemented in Gaussian 09.[23] The geometry optimization was carried out in both the gaseous phase and the reaction field of acetonitrile with the polarizable continuum model together with the UAKS parameter set. To calculate the energy barrier for the fluorination, reaction paths were constructed by varying a distance between the fluoride and the respective ipso aryl carbon in the *GS* in increments of 0.1 Å while relaxing the rest of the structure in the gaseous phase. The geometries of the *TS*s were further optimized in the reaction field of acetonitrile and a single imaginary frequency was obtained for each *TS*.

^{19}F-NMR spectroscopy. ^{19}F NMR chemical shifts were verified by comparison with authentic samples.

Acknowledgments. This study was supported by the Intramural Research Program of the National Institutes of Mental Health (NIMH: ZIA-MH002793) and the Center for Information Technology (CIT: ZIA-CT000265-20) and W. J. Youngs (Chemistry Department, University of Akron) acknowledge the National Science Foundation (CHE-0116041) and the Ohio Board of Regents for funds used to purchase the Bruker-Nonius Apex CCD X-ray diffractometer used in this research. The quantum chemical study utilized PC/LINUX clusters at the Center for Molecular Modeling (CMM) of the NIH (http://cmm.nih.gov). YS Lee thanks Dr. Sergio Hassan of the CMM/CIT for helpful discussion.

Supporting Information Available: CCDC-776799 (**1a**) and CCDC-776798 (**2a**) contain the supplementary crystallographic data for this paper. These data can be obtained free of charge from The Cambridge Crystallographic Data Centre via www.ccdc.ac.uk/data_request/cif. Detailed experimental procedures, product characterization, and tables of crystallographic data. This material is available free of charge.

References

[1] a) E. A. Merritt, B. Olofsson, *Angew. Chem. Int. Ed*. **2009**, *48*, 9052–9070. b) V. V. Zhdankin, Hypervalent Iodine Chemistry, Wiley, **2013**. c) K. Aradi, B. L. Töth, G. L. Tolnai, Z. Novák, *Synlett* **2016**, *27*, 1456–1485. d) B. Olofsson, *Top Curr. Chem.* **2016**, *373*, 135−166. e) Y. Akira, V. V. Zhdankin, *Chem. Rev*., **2016**, *116*, 3328−3435.

[2] a) F. M. Beringer, A. Brierley, M. Drexler, E. M. Grindler, C. C. Lumpkin, *J. Am. Chem. Soc*. **1953**, *75*, 2708−2712. b) F. M. Beringer, E. M. Grindler, *J. Am. Chem. Soc*. **1955**, *77*, 3203–3207. c) F. M. Beringer, M. Mausner, *J. Am. Chem. Soc.* **1958**, *80*, 4535–4536. d) Y. Yamada, K. Kashima, M. Okawara, *Bull Chem. Soc. Jap*. **1974**, *47*, 3179−3180. e) Y. Yamada, K. Konhima, M. Okawara. *Bull. Chem. Soc. Jap*. **1977**, *47*, 3179−3180. f) J. J. Lubinkowski, M. Gomez, J. L. Calderon, W. E. McEwan, *J. Org. Chem.* **1978**, *43*, 2432–2435. g) M. A. Carroll, R. A. Wood, *Tetrahedron* **2007**, *63*, 11349–11354. h) M.-R. Zhang, K. Kumata, M. Takei, T. Fukumura, K. Suzuki, *Appl. Radiat. Isot.* **2008**, *66*, 1341–1345. i) Y. Kakinuma, K. Moriyama, H. Togo, *Synthesis* **2013**, *45*, 183−188. j) J. Xu, P. Zhang, Y. Gao, Y. Chen, G. Tang, Y. Zhao, *J. Org. Chem.* **2013**, *78*, 8176–8183. k) J. Malmgren, S. Santoro, N. Jalalian, F. Himo, B. Olofsson, *Chem.-A Eur. J.* **2013**, *19*, 10334–10342. l) M. E. Hirschberg, P. Barthen, H.-J. Frohn, D. Bläser, B. Tobey, G. Jansen, *J. Fluorine Chem.* **2014**, *163*, 28–33. m) F. Guérard, Y.-S. Lee, K. Baidoo, J.-F. Gestin, M. W. Brechbiel, *Chem.-A Eur. J.* **2016**, *22*, 12332–12339.

[3] a) V. W. Pike, F. I. Aigbirhio, *J. Chem. Soc., Chem. Commun.* **1995**, *21*, 2215–2216. b) L. Ross, J. Ermert, C. Hocke, H. H. Coenen, *J. Am. Chem. Soc.* **2007**, *129*, 8018–8025. c). J.-H. Chun, S. Lu, Y.-S. Lee, V. W. Pike, *J. Org. Chem.* **2010**, *75*, 3332–3338.

[4] a) M. Phelps, J. Mazziotta, H. Schelbert, *Positron Emission Tomography and Autoradiography: Principles and Applications for the Brain and Heart*, Raven Press, New York, **1986**. b) M. E. Phelps, *Proc. Natl. Acad. Sci. U. S. A.* **2000**, *97*, 9226–9233.

[5] a) L. Cai, S. Lu, V. W. Pike, *Eur. J. Org. Chem.* **2008**, 2853–2873. b) E. L. Cole, M. N. Stewart, R. Littich, R. Hoareau, P. J. H. Scott, *Curr. Topics Med. Chem.* **2014**, *14*, 875–900. c) M. G. Campbell, T. Ritter, *Chem. Rev.* **2015**, *115*, 612−633. d) S. Preshlock, M. Tredwell, V. Gouverneur. *Chem. Rev.* **2016**, *116*, 719−766.

[6] For a recent review of the application of this labeling methodology see: M. S. Yusubov, D. Y. Svitich, M. S. Larkina, V. V. Zhdankin, *ARKIVOC* **2013** (i), 364–395.

[7] For examples of radiotracers, see: a) S. Telu, J.-H. Chun, F. G. Siméon, S. Lu, V. W. Pike, *Org. Biomol. Chem.* **2011**, *9*, 6629–6638. b) B. S. Moon, H. S. Kil, J. H. Park, J. S. Kim, J. Park, D. Y. Chi, B. C. Lee, S. E. Kim, *Org. Biomol. Chem.* **2011**, *9*, 8346–8355. c) S. V. Selivanova, T. Stellfeld, T. K. Heinrich, A. Müller, S. D. Krämer, P. A. Schubiger, R. Schibli, S. M. Ametamey, B. Vos, J. Meding, M. Bauser, J. Hütter, L. M. Dinkelborg, *J. Med. Chem.* **2013**, *56*, 4912–4920. d) K. S. Jang, Y.-W. Jung, G. Gu, R. A. Koeppe, P. S. Sherman, C. A. Quesada, D. M. Raffel, *J. Med. Chem.* **2013**, *56*, 7312–7323. e) R. Xu, P. Zanotti-Fregonara, S. S. Zoghbi, R. L. Gladding, A. E. Woock, R. B. Innis, V. W. Pike, *J. Med. Chem.* **2013**, *56*, 9146–9155. f) B. S. Moon, J. H. Park, H. J. Lee, B. C. Lee, S. E. Kim, *Mol. Imaging Biol.* **2014**, *16*, 619–625. g) R. Edwards, A. D. Westwell, S. Daniels, T. Wirth, *Eur. J. Org. Chem.* **2015**, 625−630. h) K. D. Neumann, L. Qin, A. L. Vavere, B. Shen, Z. Miao, F. T. Chin, B. L. Shulkin, S. E. Snyder, S. G. DiMagno, *J. Label. Compd. Radiopharm.* **2016**, *59*, 30−34. i) C. Warnier, C. Lemaire, G. Becker, G. Zaragoza, F. Giacomelli, J. Aerts, M. Otabashi, M. A. Bahri, J. Mercier, A. Plenevaux, A. Luxen, *J. Med. Chem.* **2016**, *59*, 8955−8966.

[8] For examples of labeling synthons, see a) J. Ermert, C. Hocke, T. Ludwig, R. Gail, H. H. Coenen. *J. Label. Compd. Radiopharm.* **2004**, *47*, 429−441. b) F. Basuli, H. Wu, G. L. Griffiths. *J. Label. Compd. Radiopharm.* **2011**, *54*, 224−228. c) J.-H. Chun, V. W. Pike, *Chem. Commun*. **2012**, *48*, 9921−9923. d) J.-H. Chun, V. W. Pike, *Eur. J. Org. Chem.* **2012**, 4541−4547. e) J.-H. Chun, V. W. Pike, *Org. Biomol. Chem.* **2013**, *11*, 6300−6306.

[9] a) M. Ochiai, Y. Kitagawa, M. Toyonari, *ARKIVOC*, **2003**, (vi) 43−48. b) M. Ochiai, *Hypervalent Iodine Chemistry: Modern Developments in Organic Synthesis* (ed. T. Wirth), Springer Verlag, Berlin. *Top. Curr. Chem*. **2003**, *224*, 5−67.

[10] a) A. Shah, V. W. Pike, D. A. Widdowson, *J. Chem. Soc. Perkin Trans. 1* **1997**, 2463−2465. b) V. W. Pike, F. Butt, A. Shah, D. A. Widdowson, *J. Chem. Soc., Perkin Trans. 1* **1999**, 245−248. c) M. A. Carroll, V. W. Pike, D. A. Widdowson, *Tetrahedron Lett*. **2000**, *41*, 5393−5396. d) M. Bielawski, B. Olofsson, *Chem. Commun*. **2007**, 2521−2523. e) M. Bielawski, M. Zhu, B. Olofsson, *Adv. Synth. Catal*. **2007**, *140*, 2610−2618. f) M. Zhu, N. Jalalian, B. Olofsson, *Synlett*, **2008**, 592−596. g) M. Bielawski, D. Alli, B. Olofsson, *J. Org. Chem.* **2008**, *73*, 4602−4607. h) M. Bielawski, B. Olofsson, *Org. Synth*. **2009**, *86*, 308−314. i) J.-H. Chun, V. W. Pike, *J. Org. Chem.* **2012**, *77*, 1931−1938.

[11] a) A. Shah, V. W. Pike, D. A. Widdowson, *J. Chem. Soc., Perkin Trans. 1* **1998**, 2043–2045. b) J.-H. Chun, S. Lu, V. W. Pike, *Eur. J. Org. Chem.* **2011**, 4439–4447. c) J.-H. Chun, S. Telu, S. Lu, V. W. Pike, *Org. Biomol. Chem*. **2013**, *11*, 5094–5099.

[12] a) Y. Yamada, M. Okawara, *Bull. Chem. Soc. Jap.* **1972**, *45*, 1860–1863. b) K. M. Lancer, G. H. Wiegand, *J. Org. Chem.* **1976**, *41*, 3360–3364.

[13] a) M. A. Carroll, S. Martín-Santamaría, V. W. Pike, H. S. Rzepa, D. A. Widdowson, *J. Chem. Soc., Perkin Trans. 2*, **1999**, 2707–2714. b) S. Martín-Santamaría, M. A. Carroll, V. W. Pike, H. S. Rzepa, D. A. Widdowson, *J. Chem. Soc., Perkin Trans. 2*, **2000**, *2*, 2158–2161. c) S. Martín-Santamaría, M. A. Carroll, C. M. Carroll, C. D. Carter, V. W. Pike, H. S. Rzepa, D. A. Widdowson. *Chem.*

Commun. **2000**, 649−650. d) H. Pinto de Magalhaes, H. P. Luthi, A. Togni, *Org. Lett.* **2012**, *14*, 3830–3833. e) D. E. Hill, J. P. Holland, *Comput. Theor. Chem*. **2015**, *1066*, 34–46.

[14] a) N. W. Alcock, R. M. Countryman, *J. Chem. Soc. Dalton Trans*. **1977**, 217–219; b) N. W. Alcock, R. M. Countryman, *J. Chem. Soc., Dalton Trans.* **1987**, 193–196. c) H. Li, S. Jiang, *Acta Cryst.* **2007**, E63, o83–o85. d) C. Y. Liu, H. Li, A.-G. Meng, *Acta Cryst.* **2007**, E63, o3647. e) Y.-S. Lee, M. Hodošček, J.-H. Chun, V. W. Pike, *Chem.-A. Eur. J.* **2010**, *16*, 10418–10423.

[15] K. Chen, G. F. Koser, *J. Org. Chem.* **1991**, *56*, 5764–5767.

[16] R. D. Burbank, G. R. Jones, *Science* **1970**, *168*, 248–249.

[17] C. Ye, B. Twamley, J. M. Shreeve, *Org. Lett.* **2005**, *7*, 3961–3964.

[18] (a) I. Haiduc, *Coord. Chem. Rev*. **1997**, *158*, 325−358. b) G. A. Landrum, N. Goldberg, R. Hoffmann, R. M. Minyaev. *New J. Chem*. **1998**, 883−890.

[19] J. I. Seeman, *Chem. Rev.* **1983**, *83*, 83–134.

[20] a) C.-G. Zhan, D. A. Dixon, *J. Phys Chem. A* **2004**, *108*, 2020–2029. b) M. A. Vincent, I. H. Hillier, *Chem. Commun*. **2005**, 5902–5903.

[21] Y. B. Yu, P. L. Privalov, R. S. Hodges, *Biophys. J.* **2001**, *81*, 1632–1642.

[22] M. Ochiai, M. Kida, K. Sato, T. Takino, S. Goto, N. Donkai, T. Okuyama, *Tetrahedron Lett*. **1999**, *40*, 1559–1562.

[23] J. Frisch, G. W. Trucks, H. B. Schlegel, G. E. Scuseria, M. A. Robb, J. R. Cheeseman, G. Scalmani, V. Barone, B. Mennucci, G. A. Petersson, H. Nakatsuji, M. Caricato, X. Li, H. P. Hratchian, A. F. Izmaylov, J. Bloino, G. Zheng, J. L. Sonnenberg, M. Hada, M. Ehara, K. Toyota, R. Fukuda, J. Hasegawa, M. Ishida, T. Nakajima, Y. Honda, O. Kitao, H. Nakai, T. Vreven, J. A. Montgomery, Jr., J. E. Peralta, F. Ogliaro, M. Bearpark, J. J. Heyd, E. Brothers, K. N. Kudin, V. N. Staroverov, R. Kobayashi, J. Normand, K. Raghavachari, A. Rendell, J. C. Burant, S. S. Iyengar, J. Tomasi, M. Cossi, N. Rega, J. M. Millam, M. Klene, J. E. Knox, J. B. Cross, V. Bakken, C. Adamo, J. Jaramillo, R. Gomperts, R. E. Stratmann, O. Yazyev, A. J. Austin, R. Cammi, C. Pomelli, J. W. Ochterski, R.

L. Martin, K. Morokuma, V. G. Zakrzewski, G. A. Voth, P. Salvador, J. J. Dannenberg, S. Dapprich, A. D. Daniels, Ö. Farkas, J. B. Foresman, J. V. Ortiz, J. Cioslowski, D. J. Fox, Gaussian 09, revision A.02, Gaussian Inc., Wallingford CT, **2009**.

Captions

Figure 1. Examples of a) radiolabeling synthons and b) prominent PET radiotracers produced directly by the radiofluorination of diaryliodonium salts.

Scheme 1. General scheme for the reaction between diaryiodonium salts and nucleophiles.

Figure 2. Diaryliodonium salts discussed and referred to in this study.

Figure 3. Crystal structure of **1a** together with the two water and two acetonitrile molecules from the crystallization solvent. Both bond lengths and H-bonding distances are shown in Å. Carbon atoms are shown in green, hydrogen atoms in white, oxygen atoms in red, iodine atoms in violet, nitrogen atoms in dark blue and fluorine atoms in gray. Blue distances are I···F bonds; red distances are H bonds. Since the unit cell has the center of inversion, only non-redundant bond distances are sho
wn. The inset gives a formulaic planar view of the structure with water and acetonitrile molecules omitted.

Figure 4. Crystal structure of **2a**. Hydrogen bonding interactions for three water molecules above and three watermolecules below the plane of the two iodine and two fluorine atoms are indicated by their respective yellow dashed lines. Carbon atoms are shown in green, hydrogen atoms in white, oxygen atoms in red, iodine atoms in violet, and fluorine atoms in gray. Blue distances are I−F bonds; red distances are H bonds; green distance is an exocyclic I−F bond. All distances are in Å. The unit cell has the center of inversion and thus only non-redundant bond distances are given. The inset gives a formulaic planar view of the structure without water molecules.

Figure 5. Overlay of the crystal structures of **1a** (dark blue) and **2a** (yellow); **2a** was superimposed with the best fit by using the four iodine and four fluorine atoms of **1a** as the common docking point. Hydrogen atoms and solvent molecules are not shown.

Figure 6. Reverse phase radio-HPLC chromatogram of the crude product from the radiofluorination of **2a**.

Figure 7. A) ^{19}F-NMR spectrum for **2a** in DMSO-d_6. B). ^{19}F NMR spectrum of the crude product from the thermal decomposition of **2a** in DMSO-d_6 at 100 ^{o}C for 10 min, showing the two fluoroarene products, fluorobenzene and *o*-fluorotoluene.

Figure 8. Reaction path for the thermolysis of monomeric **2a** in acetonitrile. Labeled bond distances are shown in Å. Carbon atoms are shown in green, hydrogen atoms in white, iodine atoms in violet, and fluorine atoms in yellow. Dashed red lines and numbers are distances between the fluoride ion and the nearest carbon atom ipso to the iodine atom. TS_A leads to fluorobenzene and TS_B to *o*-fluorotoluene.

Figure 9. Structures of *GS*s and *TS*s of diphenyliodonium fluoride (**1a**) in dimeric, heterodimeric and tetrameric states. All distances are in Å. Carbon atoms are shown in green, hydrogen atoms in white, iodine atoms in violet, chlorine atoms in red, and fluorine atoms in yellow. The coordinates of these structures are given in the Supporting Information.

Figure 10. Reaction path for the fluorination of **1a**/**1b**. The more stable dimer is in equilibrium with its monomers, and the interconversion between the two is assumed to be much faster than the fluorination itself. The TS_M and TS_D

represent the *TS* of fluorination in monomeric and dimeric conformations, respectively, and their energy levels are depicted with respect to the *GS* of dimer (GS_D); TS_M energy level is the sum of the ΔGS_D and $\Delta G_M^{\ddagger}$ values of the monomeric **1a**. The TS_M of the heterodimeric conformation does not show Ph_2ICl.

Table of Contents

FULL PAPER

The 'ortho effect' imparted by an *o*-alkyl group in the reaction of diarylodonium salts with fluoride ion is attributed to a favorable electrostatic interaction between the incoming fluoride and the *o*-methyl group in the transition state (TS_B).

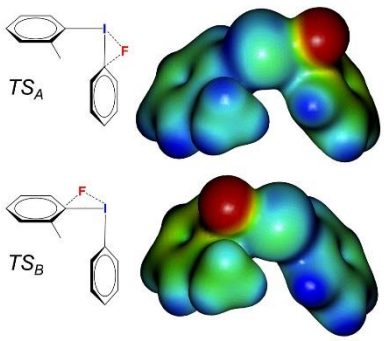

Y.-S. Lee, J.-H. Chun, M. Hodošček, and V.W. Pike*

Page No. – Page No.

Crystal Structures of Diaryliodonium Fluorides and their Implications for Fluorination Mechanisms

Key Words: radiofluorination; chemoselectivity; orhto-effect; quantum chemistry; monomeric vs oligomeric reaction pathway